3

Improving stability of Pb and Sn-based absorber layer through microstructure control

3.1 Broad Context

One of the major concerns with perovskite solar cells (PSCs) is achieving compact and large-grained microstructure of the perovskite film, as poor microstructure leads to the instability of the perovskite film in presence of moisture and air. Microstructure of films is one of the fundamental criterions for achieving better stability and performance of solar cell, because many photo-physical properties, such as light harvesting, charge carrier transport and diffusion length, can be affected by the crystallization of the perovskite [129]. Moreover, defects and the crystal grain boundaries of the perovskite crystallites act as the traps of carriers, which aggravate the charge recombination. The hysteresis effect, which is very much common in PSCs causes inaccuracy in evaluating cell efficiency, is also believed to be related to the crystallinity and interfaces of the perovskite. Thus, the device performance strongly depends on the microstructure of the perovskite film [130].

3.2 Introduction

In recent years PSC have gained wide acceptance in the photovoltaic (PV) community owing to their fascinating optoelectronic properties such as high absorption coefficient, long charge-carrier diffusion lengths, high defect tolerance low cost and ease of fabrication. Recently, PSCs has achieved a record PCEs of over 26% [33,131]. Long-term stability is a major hurdle to be surpassed for the commercialization of PSCs. The instability of PSCs is mainly attributed to the degradation of the perovskite layer and/or other functional layers under external factors

such as oxygen, moisture, heat, light, electric bias, etc. [132–134]. During the processing, poor perovskite films with low coverage, pores, and small grain size are often obtained. All these issues lead to the easy decomposition of films in the environment and lowers the PCE. A fast nucleation rate and low crystallinity are the main reasons for the poor film quality. Therefore, in order to obtain high-quality films, the primary requirement is to control the factors that affect the evolution and growth of perovskite layer. Here, we have explored the factors that may affect the growth of the perovskite films during processing.

3.3 Additive Engineering

In the solution-processed method (SPM) a precursor solution i.e. mixing PbX_2 (X = Cl, I, Br) and AX (A = MA, FA) into a polar solvent like N, N-dimethylformamide (DMF), dimethyl sulfoxide (DMSO) or gamma-butyrolactone (GBL) is spin coated onto a substrate to form a perovskite film which is further annealed to converts into perovskite film by removing the residual solvent [135]. However, microstructure control (uniformity, coverage, and roughness) of the perovskite film is the biggest challenge with solution-processed PSCs, as the photo-physical properties, such as light harvesting, charge carrier transport and diffusion length, can be changed with the crystallization (is related to nucleation and growth) of the perovskite [136–138].

One or two-step spin-coating is the most commonly used synthesis technique for perovskite absorber layers. In one step spin coating process, PbX_2 (X = Cl, I, Br) and AX (A=MA, FA) are dissolved into a polar solvent such as DMF or DMSO, forming several adducts which on annealing converts to perovskite phase [139]. The precursor solution is spin coated on the substrate for a few seconds, followed by an anti-solvent (toluene or CB) dripping to remove excess solvent [140]. The polar solvents (DMSO and DMF) act as Lewis bases and PbX_2 (X = Cl, I, Br) as Lewis acids forming acid–base adducts during spin coating, which decomposes to

form perovskite on annealing. The crystallization and microstructure of perovskite films depend on the rate of decomposition and bonding characteristic of these adducts [139,141].

In the case of Sn-based perovskite, the microstructure of films is dictated by their fast nucleation and growth kinetics. Therefore, the most straightforward approach for improving the film microstructure is to control the crystallization kinetics during processing. Adding tin-halide (SnF_2 or $SnCl_2$) as an antioxidant in the solution has shown some promising results [142]. The addition of SnF_2 reduces the concentration of Sn vacancy (V_{sn}) by increasing its formation energy, serves as heterogeneous nucleation sites, and facilitates the formation of more Sn-based perovskite nuclei thereby, enhancing the homogeneous crystal growth resulting in uniform film coverage [143].

3.4 Solvent Engineering

In SPM, solvent not only dissolves the precursor but also participates in the crystallization of perovskite, as polar solvents (DMSO, DMF) act as Lewis bases (electron pair donors) and PbX_2 (X = Cl, I, Br) as Lewis acids (electron pair acceptors), which form Lewis acid–base adducts (intermediate phase) to delay the crystallization rate and passivating the grain boundaries. Whereas antisolvents (CB, toluene and diethyl ether) not only remove the excess solvent in the precursor but also increase the saturation rate in the precursor solution, resulting in the rapid and uniform nucleation of the perovskite to form dense and smooth films [139]. Secondly, the substrate materials help in controlling the nucleation and growth of films as different substrate materials will affect the wettability and distribution of the precursor and ultimately affect the microstructure of the film [144]. Lastly, annealing is an important step in where some solvents or additives are removed which promotes the growth of crystal grains; and ensures the crystallization of the perovskite, by removing the solvent on the surface [141].

Dripping of an anti-solvent such as CB, toluene and diethyl ether during spin coating has also been reported to help in improving the quality of the films and allow good coverage of the substrate [82].

3.5 Evolution of Microstructure in Pb based perovskite absorber layer

The reported efficiency (>26%) of PSC has surpassed that of Si solar cells mainly because of its high absorption coefficient, long charge-carrier diffusion length, and high defect tolerance [33]. However, the long-term stability of the perovskite absorber layer in the ambient atmosphere is still a major concern. Formamidinium lead iodide ($FAPbI_3$) is the most studied Pb-based perovskite material. The hexagonal δ-phase (P63m, yellow phase) of $FAPbI_3$ is thermodynamically stable at room temperature, while the most suitable tetragonal/trigonal (P3m1) α-phase (black phase) is stable at temperatures above 160°C. Partial substitution of methylammonium ions (MA^+) with large dipole moment into $FAPbI_3$ structure stabilizes the α-$FAPbI_3$ at lower temperatures [57]. On the other hand, incorporating MABr into $FAPbI_3$ widens the bandgap, enhancing thermal stability and open circuit voltage (V_{oc}) [145].

The stability, photo-carrier generation, and large carrier transport depends on the grain size, microstructure and compactness of the films, which in turn is decided by the adduct formation and annealing parameters. Here we have utilized radiative annealing at (RA) 120 ºC to achieve a compact and large-grained perovskite ($FA_{0.75}MA_{0.25}Pb(BrI)_3$) absorber layer and demonstrated its stability for up to 60 days in ambient conditions.

A small amount of methyl bromide (MABr) was added to increase open circuit voltage (V_{oc}) and to enhance the structural stability of the $FAPbI_3$ α-phase [57,145]. The experimental procedure for TiO_2, SnO_2 and perovskite ($FAMAPb(BrI)_3$ is mentioned in Chapter 2. It is observed that the film ($FA_{0.75}MA_{0.25}Pb(BrI)_3$) prepared with DMF alone as solvent was not dense and comprised of multiple pinholes (**Figure 3.1a**). The poor microstructure is ascribed

to the fact that DMF exhibits retrograde solubility (or inverse solubility behaviour) for bromide, which promotes $(MA)_2Pb_3I_{8-\delta}Br_\delta \cdot 2DMF$ adduct formation [146] and results in phase segregation of iodide and bromide species [147,148]. On the other hand, DMSO does not shows inverse solubility for Br counterparts because of its larger donor number (quantitative measure of Lewis basicity) of 29.8 which is greater than that of DMF (26.6). Therefore, MABr mix well in DMSO and forms both the iodide and bromide species together [147]. Moreover, lone pair electrons of oxygen in DMSO interact with Pb^{2+} in PbI_2 to form adducts that are stronger than the DMF adducts. Using DMSO as a co-solvent along with DMF (in 1:4 ratios) delays the decomposition of adducts and crystallization of the perovskite phase, thereby controlling the irregular grain growth and microstructure. Dripping of anti-solvent CB removes the residual solvents during the third stage of spin coating, making it supersaturated. On annealing, it results in uniform nucleation and the formation of dense film [140]. The F$AMAPb(BrI)_3$ films were prepared on TiO_2 and SnO_2 substrates and initially annealed at 100 ºC for 10 minutes to study the role of the substrate on the film microstructure. Although both films had small grain structures and pinholes, the film deposited on the SnO_2-coated substrate was comparatively uniform while TiO_2 had some porosity and was not clearly dense (**Figure 3.1b** and **c**). This is likely because of the greater wettability of perovskite solution on SnO_2 (contact angle≈10.33°) when compared to that of TiO_2 (contact angle≈30°) surface. Therefore, SnO_2-coated FTO was chosen as a substrate to further improve the microstructure. To ensure perovskite nucleation in the early stages, during spin coating, an IR lamp (power 150 Watt) was installed directly above the spin coater to facilitate evaporation of solvent during adduct formation and quick super saturation. However, IR lamp do not result in controlled nucleation and bigger grains; rather it formed streak-like microstructure with tiny grains (**Figure 3.1d**). It is concluded that the nucleation and growth should be controlled without disturbing the adduct formation. For achieving large grained microstructure rate of solvent release from adduct should be slightly

faster than that of evaporation. Therefore, IR lamp was removed and the annealing temperature was raised to 120 ºC for 1 hour to evaporate solvent and facilitate the conversion of adduct phases into perovskite. Annealing at 120 ºC for 1 hour did mitigate the streak formation; however, resulted in irregular grain and crack formation (**Figure 3.1e**) which could be due to prolonged exposure at 120 ºC. To avoid crack formation, and ensure grain growth, annealing at higher temperatures (up to 250 ºC) for shorter duration has been reported [149]. Here, we have employed radiative annealing (RA) at 120°C for 1 minute in inert (RAI) and vacuum (RAV) conditions. During RA, radiative heat is absorbed preferentially by the top layer while the substrates remain largely unaffected due to short exposure times [150]. RAI quickens the solvent evaporation rate and improves the film crystallization process. **Figure 3.1f-g** depicts microstructure of the RAI and RAV films. RA films are relatively more compact than the films processed on hot plates. RAI had relatively small grains, while RAV films are compact having larger gains (**Figure 3.1g**). Simultaneous vacuum while heating during RAV resulted in faster release and volatilization of by-products/solvents hastening the perovskite crystallization from the adduct, an effect which was earlier achieved by heating to higher temperatures [149,151].

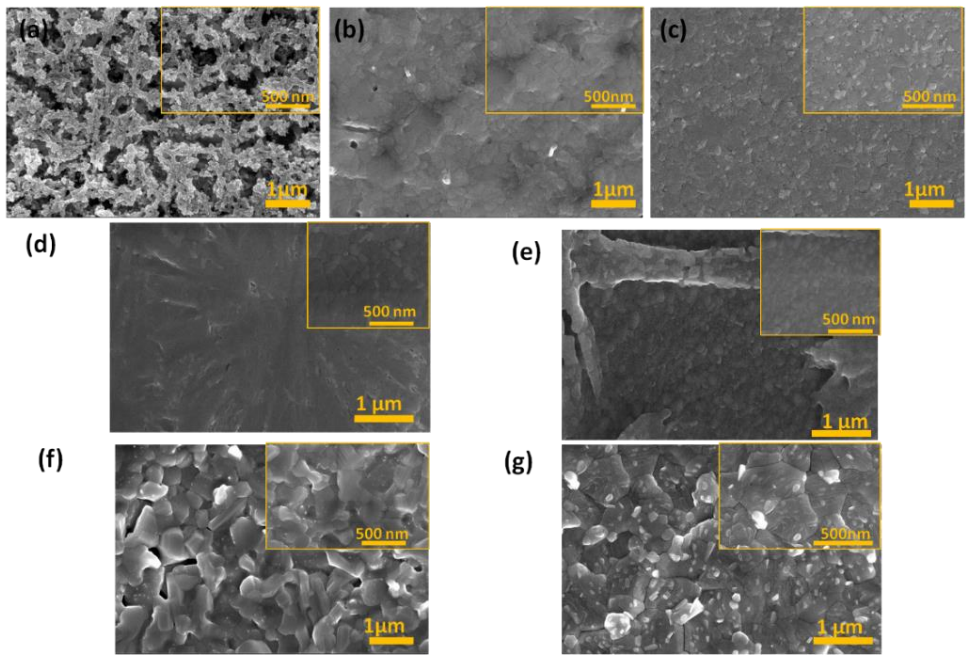

Figure 3.1 SEM images of FAMAPb(BrI)$_3$ film with a) DMF only b) DMF+DMSO+CB dripping on TiO_2 , c) on SnO_2, d) heated on 100°C with IR e) 120 °C without IR lamp, RA at 120 °C f) inert g) in vacuum.

The degradation of the deposited perovskite films was monitored as a function of time (**Figure 3.2a**). Both RAI and RAV films exhibit relatively greater stability when compared to the other films. RAV film remains black even after 60 days in ambient conditions (RH≈60%), while the other films became yellow or translucent within 20-45 days. All the major peaks of the XRD pattern of RAV film could be indexed to crystallographic planes of $FA_{0.75}MA_{0.25}Pb(BrI)_3$ [152]. The relatively smaller peaks at 11.06° and 12.40° are assigned to the δ-$FAPbI_3$ and PbI_2 phases. PbI_2 and δ-$FAPbI_3$ present in the freshly prepared film is probably due to minor phase segregation [148]. There is only marginal increase in the intensity of PbI_2 and δ-$FAPbI_3$ peaks, while the major peaks belonging to $FA_{0.75}MA_{0.25}$ $Pb(BrI)_3$ gradually decreases with respect to the fresh sample (**Figure 3b**), although the film remains black in colour (**Figure 3a**). This suggests that the film has started to degrade however, a measurable amount of the perovskite phase is still intact and the observed rise in PbI_2 peaks is due to the formation of halide vacancy and segregation of PbI_2. The presence of peak at $FA_{0.75}MA_{0.25}Pb(BrI)_3$ peaks albeit with lower intensity even after 60 days in ambient conditions (RH 60%) confirms relatively better stability of RAV films.

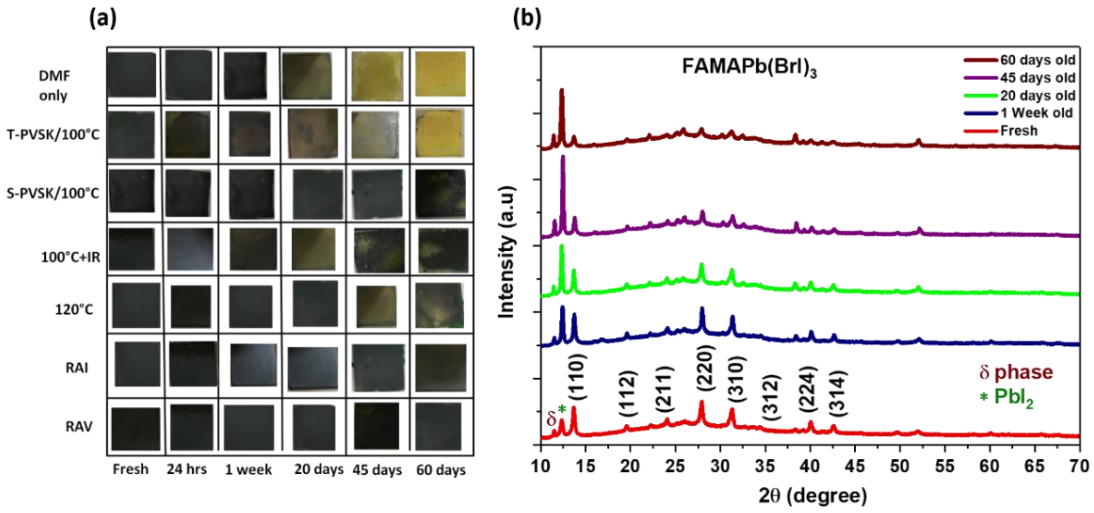

Figure 3.2 Comparison of color change in FAMAPb(I,Br)$_3$ films, and b) XRD patterns of RAV films as a function of time.

Band gap of 1.53 eV is calculated from the UV-vis spectroscopy (**Figure 3.3a**) using Tauc plot (inset of **Figure 3.3a**) [153]. PL peak at around 780 nm (**Figure 3.3b**) matches closely with the band gap of FAMAPb(BrI)$_3$ indicating to the band-to-band transition. PL decay curve (**Figure 3.3c**) is fitted to a bi-exponential equation ($Y=A_1\exp(-t/\tau_1)+A_2\exp(-t/\tau_2)$). The shorter decay time (τ_1~2 ns) manifests the fillings of the trap states, while the longer decay time (τ_2~12 ns) is attributed to the radiative recombination of photo-generated carriers. A relatively low average decay time (τ_{avg}) of ~7.5 ns indicates that the ETL layer (SnO_2) is effective in extraction of photo-generated electrons [154]. A solar cell was fabricated on SnO_2 and spiro-OmeTAD as ETL and HTL respectively, gold is used as electrode (detail in Chapter 2), and the active area of the device is 0.01 cm^2 (**Figure 3.3 d**) shows the J-V curve of PSC based FAMAPb(BrI)$_3$ perovskite. The measured PCE was about 12.24%, while the open circuit voltage (V_{oc}), short circuit current (J_{sc}) and FF were 0.90 V, 25 mAcm^{-2} and 55%, respectively. As expected high V_{oc} (0.90 V) is achieved because of the addition of the MABr in the $FAPbI_3$ which is used to get wide bandgap close to 1.53 eV. At the same time PCE is limited to 12% only, the relatively lower performance is

attributed to the smallest FF which is only 55%. This could be because of the undesired minor Br-rich phase segregation at the grain boundaries which cannot be easily detected from XRD.

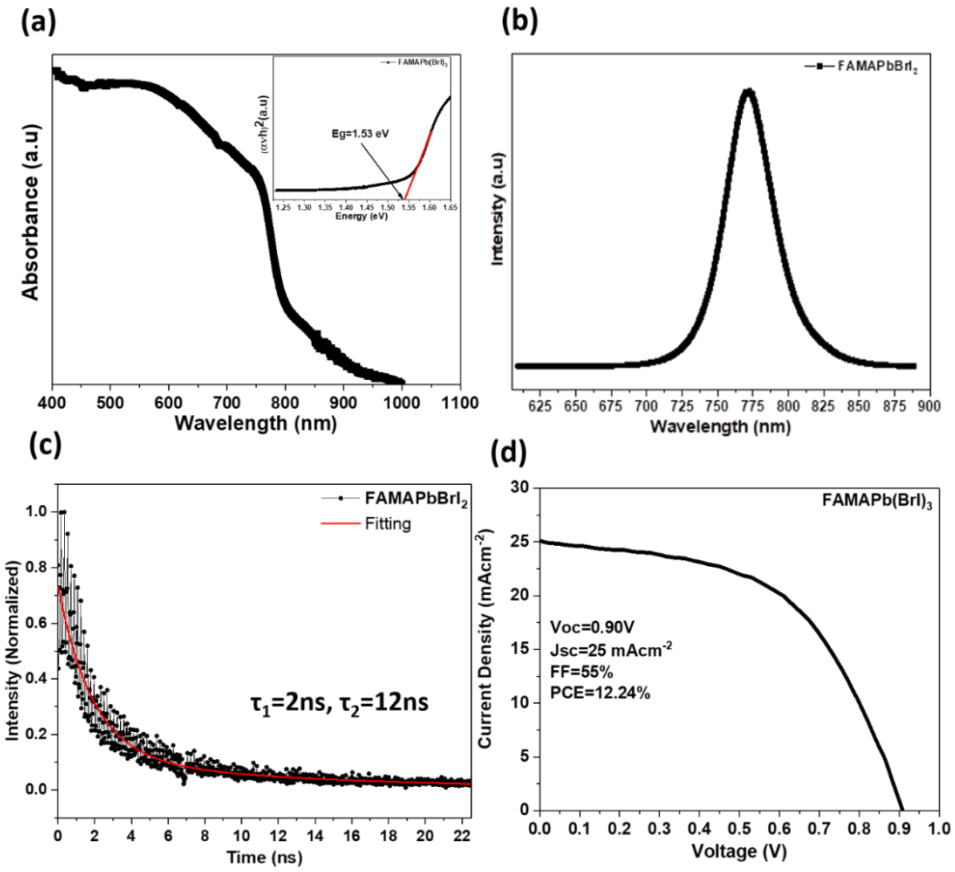

Figure 3.3. a) Absorbance and Tauc plot (inset), b) Photoluminescence and c) lifetime measurement and d) J-V curve of $FAMAPb(BrI)_3$ based perovskite solar cell.

3.6 Achieving a large grained and compact microstructure in Sn-based perovskite

Lead-based perovskite solar cells have shown tremendous progress by improving efficiency from ~4% to over 26% [32,155] in just 9-10 years. However, due to the toxicity associated with Pb, and Sn having a similar electron configuration and chemical nature, Sn-based PSC has been projected as an alternate to Pb-PSC. [37]. Sn-based perovskite possesses similar

optoelectronic properties [156,157] to Pb-based perovskite which makes it a viable non-toxic alternative. However, the progress of Sn-perovskite-based solar cell have been limited, and only ~12% PCE could be achieved till date [38]. The lower performance of the Sn-based absorber (such as formamidinium tin iodide $FASnI_3$ and methyl ammonium tin iodide $MASnI_3$) materials is mainly due to their poor stability and uncontrolled crystallization, which results in the formation of defective and porous films. $FASnI_3$ is considered to be more stable than $MASnI_3$ because of FA is a bigger cation with a more rigid perovskite structure yielding a tolerance factor (t) close to 1 [28].

Several reports on different types of perovskite materials have been published on controlling the crystallization and reducing degradation by utilizing SnX_2 (as a reducing agent) and anti-solvents such as toluene, diethyl ether, and CB [158,159]. Significant improvement in the film microstructure has been demonstrated by incorporating additives (SnX_2) and solvent engineering (dripping of antisolvents). The addition of SnF_2 increases the formation energy of Sn-vacancy (V_{Sn}), while at the same time, serving as uniformly distributed heterogeneous nucleation sites for the perovskite phase resulting in the homogeneous film [87,158,160]. Several reports suggest that $SnCl_2$ and SnF_2 both can be utilized as reducing agents to improve the microstructure and stability, and along with the dripping of the anti-solvents toluene, CB the microstructure can be improved further and thereby performance of PSCs. However, all these reports are on the different perovskite systems, including $CsSnI_3$, $(FA,MA)SnI_3$ and $MASnI_3$ [158,159,161] There is hardly any report concentrating on their relative effectiveness on the $FASnI_3$ perovskite system.

Here, we are reporting a comparative efficacy of the different halides SnF_2 and $SnCl_2$ in conjunction with the antisolvents (toluene and CB) in controlling the microstructure. The detailed experimental process is mention in Chapter 2. The films deposited using a precursor

with DMF solvent resulted in discontinuous microstructure having poor coverage (**Figure 3.4a**) due to uncontrollable fast crystallization and rapid oxidation of Sn^{2+} to Sn^{4+}. The presence of open pores and discontinuities allowed the moisture to easily penetrate, resulting in faster degradation of the films within 10 hours. The annealed films turned almost from black, in the as-deposited state, to yellow to almost transparent in a short span of 10 hours (shown in **Figure 3.4b**). When the coordinating solvent DMSO was added in the ratio of 1:4 (DMSO: DMF) in the precursor solution, a much improved film microstructure was obtained (**Figure 3.4c**). This was due to the formation of SnI_2.3DMSO complex, which retarded the crystallization of $FASnI_3$ and held the SnI_2 and FAI from reacting during spin-coating, resulting in uniform spread of precursor on the substrate, which on annealing resulted in films with improved coverage. Excess tin halide ($SnCl_2$ and SnF_2) was incorporated into the precursor solution as an antioxidant. The DMSO forms a stable intermediate FAI-DMSO-SnI_2 complex while the presence of excess SnX_2 provides heterogeneous nucleation site during the annealing step. At the same time, it creates/maintains a reducing environment and excess Sn ions tend to fill the Sn-vacancies and passivates the defects thus improves the stability and microstructure of the film [162]. The SEM micrographs of the films deposited using 10% excess $SnCl_2$ and SnF_2 are depicted in **Figure 3.5a and d**, respectively. Addition of 10% of $SnCl_2$ (**Figure 3.5a**) resulted in the relatively uniform film; however, the dendritic growth having branch-like structure was observed with small pores due to the fast growth of the film (**Figure 3.5a**). In the case of SnF_2 (**Figure 3.5d**), more compact and dense film with much lesser discontinuity and pinhole was observed. The presence of bright spots in the SEM images (**Figures 3.4a and 3.4d**) was attributed to the segregation of the excess Sn-halide in both the cases; however, the bright spots were much more uniformly distributed in the case of SnF_2. This reveals that in the case of SnF_2 the growth of $FnSnI_3$ during annealing was more uniform and segregation of excess phase was uniformly distributed. In order to curb the dendritic growth, small amount of (100µl) anti-

solvents toluene and CB was dripped during the 3rd spin-coating step. Anti-solvents are miscible with DMSO while does not dissolve FAI or SnI_2. Addition of the anti-solvents during 3rd spin-coating step removes any excess DMSO thereby freezing a uniform precursor film, which on annealing, aided by heterogeneous SnF_2 nuclei results in the formation of uniform equiaxed-grained dense films [163]. The CB was found to be more effective in curbing the dendritic growth and forming dense films. Although some hint of dendritic growth could be observed in the case of excess SnF_2 with toluene dripping (shown **Figure 3.5e**), it was much denser when compared to the $SnCl_2$ added films (**Figure 3.5b**). In the case of $SnCl_2$, toluene dripping resulted in cellular type growth with lots of pores as can be observed in **Figure 3.5b**. Dripping of CB resulted in uniform coverage in both the cases of $SnCl_2$ and SnF_2 addition, (**Figures 3.5c** and **3.5 f**); however, planer growth was achieved in the case of SnF_2, as a result, a dense large-grained microstructure was achieved (shown in **Figure 3.5f**). On the other hand, in the case of $SnCl_2$ with CB, intergranular pores could still be observed as shown in **Figure 3.5c**. Film deposited with excess SnF_2 and CB dripping turns out be more stable as film did not show any sign of degradation and remained black even after 10 hour in air (**Figure 3.5g**) unlike the film without additives which degraded and became transparent by 10 hours (**Figure 3.4b**).

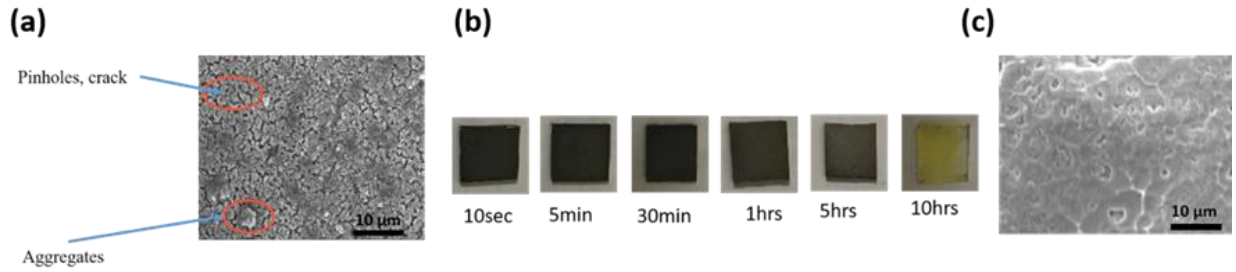

Figure 3.4 $FASnI_3$ deposited with DMF solvent b) Degradation of the film as a function of time c) Film prepared with DMF: DMSO (4:1) solvent.

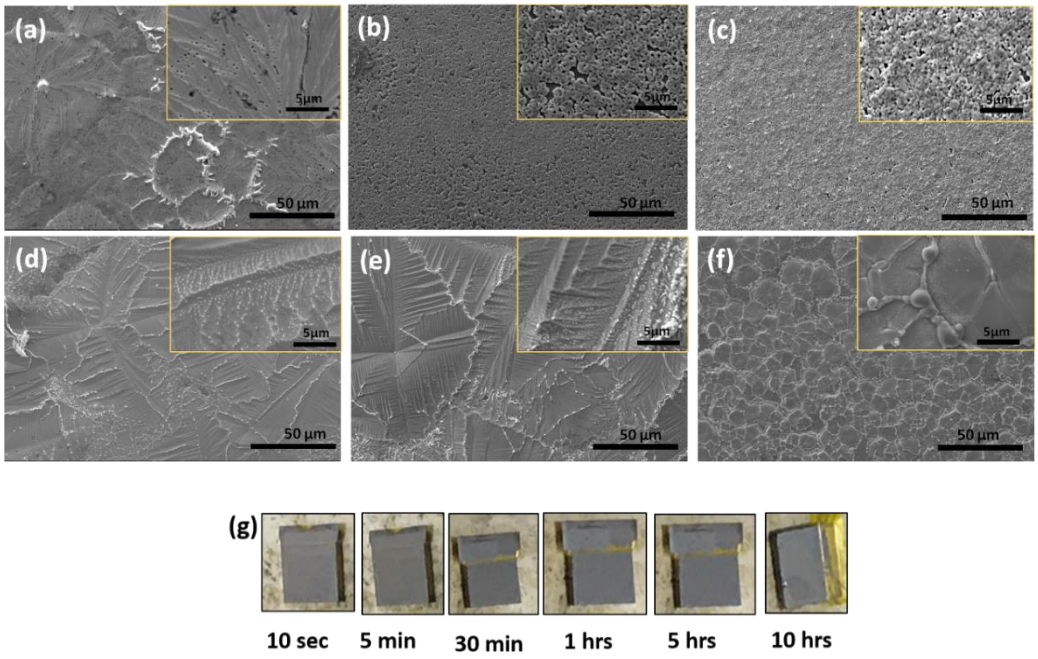

Figure 3.5 SEM images of $FASnI_3$ perovskite films on m-TiO_2 with addition a) $SnCl_2$, b) $SnCl_2$ +Toluene dripping, c) $SnCl_2$+CB, d) SnF_2 e) SnF_2+Toluene dripping, f) $FASnI_3$+SnF_2+CB dripping, and g) degradation of film prepared with the SnF_2 and CB dripping as a function of time.

Once a uniform and dense microstructure was obtained, the formation of the desired orthorhombic α-$FASnI_3$ was confirmed by XRD. The XRD pattern obtained from the CB dripped SnF_2 added film is depicted in **Figure 3.6a**. The presence of XRD peaks at 2θ positions 14°, 24.4°, 28.22°, 31.65°, 40.37° could be assigned to the crystallographic planes (100), (102), (200), (122) and (222) for α-$FASnI_3$, respectively (**Figure 3.6a**) [87]. Absence of any prominent SnF_2 peak in the XRD pattern could be because of uniformly and thinly distributed SnF_2 along the grain boundaries. UV visible spectroscopy was done to check the bandgap of the film (**Figure 3.6b**). The bandgap of 1.5eV was calculated from the Tauc plot [153] (inset of **Figure 3.6b**). which matched with the earlier reports and is suitable for the fabrication of Sn-based PSCs [37].

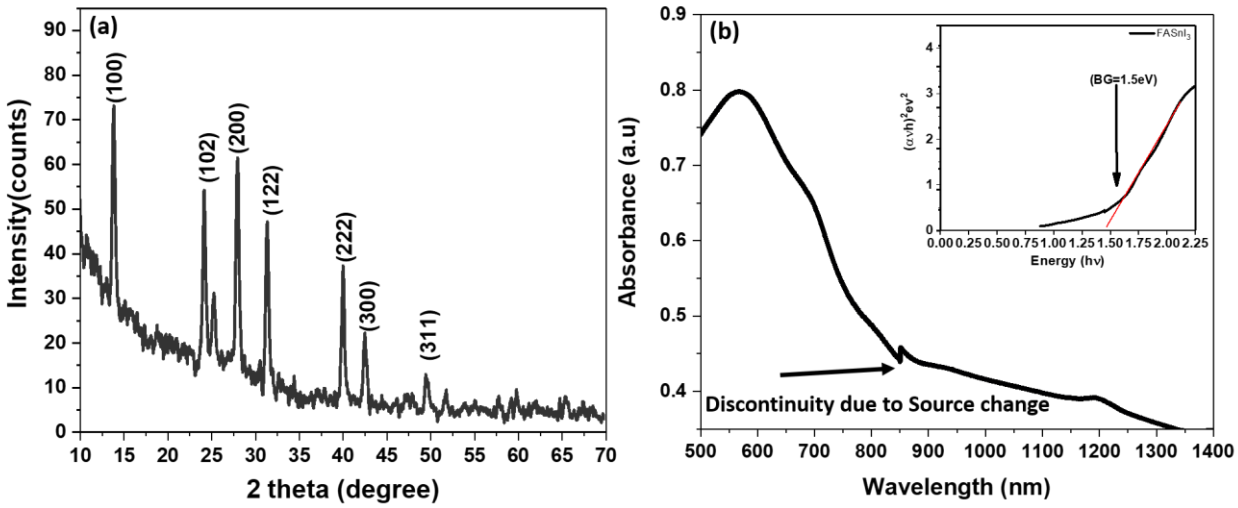

Figure 3.6 (a) XRD plot of $FASnI_3$ with 10% SnF_2 (b) UV-visible spectrum and Tauc plot (inset) of $FASnI_3$.

3.7 Conclusions

Compact $FA_{0.75}MA_{0.25}Pb(BrI)_3$ film with large grain was achieved at lower temperature (120 ^oC) using radiative annealing under vacuum (RAV) in 1 min on SnO_2 coated glass substrate using mixed solvent and CB anti-solvent. The processed film is suitable for PV absorber layers. The RAV film remained stable in 60% RH for 60 days. The bandgap of 1.53 eV and an intense band to band PL peak at around 780 nm indicates to the suitability of the films as a PV absorber layer. The PCE of device with $FAMAPb(BrI)_3$ was about 12% with SnO_2 and spiro-OMeTAD as ETL and HTL respectively.

In addition, the role of SnX_2 (X=F, Cl) and the anti-solvents (toluene and CB) on the $FASnI_3$ film microstructure were explored. The best result was obtained in the case of the antioxidant SnF_2 and anti-solvent CB. Dripping of the CB was found to be more effective in achieving uniform film in both cases 10% SnF_2 and 10% $SnCl_2$ addition. The resultant film had the desired α-$FASnI_3$ with a bandgap of ~1.5 eV, which is desirable for PV absorbers.